The human homologue of macaque area V6A ☆

S. Pitzalis [a,b,*], M.I. Sereno [c], G. Committeri [d], P. Fattori [e], G. Galati [b,f], A. Tosoni [d], C. Galletti [e]

[a] Department of Education in Sport and Human Movement, University of Rome "Foro Italico", Rome, Italy
[b] Laboratory of Neuropsychology, Santa Lucia Foundation, Rome, Italy
[c] Birkbeck and UCL Centre for Neuroimaging (BUCNI), London, UK
[d] Department of Neuroscience and Imaging and ITAB, University Gabriele d'Annunzio, Chieti, Italy
[e] Department of Human and General Physiology, University of Bologna, Bologna, Italy
[f] Department of Psychology, Sapienza University, Rome, Italy

ARTICLE INFO

ABSTRACT

In macaque monkeys, V6A is a visuomotor area located in the anterior bank of the POs, dorsal and anterior to retinotopically-organized extrastriate area V6 (Galletti et al., 1996). Unlike V6, V6A represents both contra- and ipsilateral visual fields and is broadly retinotopically organized (Galletti et al., 1999b). The contralateral lower visual field is over-represented in V6A. The central 20°–30° of the visual field is mainly represented dorsally (V6Ad) and the periphery ventrally (V6Av), at the border with V6. Both sectors of area V6A contain arm movement-related cells, active during spatially-directed reaching movements (Gamberini et al., 2011). In humans, we previously mapped the retinotopic organization of area V6 (Pitzalis et al., 2006). Here, using phase-encoded fMRI, cortical surface-based analysis and wide-field retinotopic mapping, we define a new cortical region that borders V6 anteriorly and shows a clear over-representation of the contralateral lower visual field and the periphery. As with macaque V6A, the eccentricity increases moving ventrally within the area. The new region contains a non-mirror-image representation of the visual field. Functional mapping reveals that, as in macaque V6A, the new region, but not the nearby area V6, responds during finger pointing and reaching movements. Based on similarity in position, retinotopic properties, functional organization and relationship with the neighboring extrastriate visual areas, we propose that the new cortical region is the human homologue of macaque area V6A.

© 2013 The Authors. Published by Elsevier Inc. All rights reserved.

Introduction

The visual system of non-human primates has been extensively studied using a combination of invasive methods such as tracer injections, histological stains, and single unit recordings. Thanks to non-invasive neuroimaging methods several visual areas have been mapped also in humans (for review, see Sereno, 1998; Sereno and Tootell, 2005). However, the anatomical and functional organization of important sectors of the human visual brain extensively studied in the macaque, such as the medial occipito-parietal cortex, is still poorly understood.

In monkey, the parieto-occipital sulcus (POs) contains two cytoarchitectonically and functionally distinct regions, V6 and V6A. V6 is a retinotopically organized area that represents the entire contralateral hemifield and robustly responds to unidirectional motion (Galletti et al., 1996, 1999a). V6A occupies the anterior bank of the POs, in the caudalmost part of the superior parietal lobule (Fig. 1A;

Galletti et al., 1996, 1999b). It represents both contra- and ipsilateral visual fields, but lacks a fine-grained retinotopic organization, although the central 20°–30° of the visual field is mainly represented dorsally (V6Ad) and the periphery ventrally (V6Av), where it borders area V6 (Figs. 1B–C; Galletti et al., 1999b). In V6A the contralateral lower visual field, particularly the region of the far periphery, is over-represented (Galletti et al., 1996, 1999b). Area V6A also contains many arm-movement-related cells (Fattori et al., 2001), whose activity is spatially tuned (Fig. 1D; Fattori et al., 2005) and is very sensitive to the orientation of the wrist (Fig. 1E; Fattori et al., 2009a).

In humans, we have recently described a homologue of monkey V6 in the dorsal POs using a wide-field retinotopy (Pitzalis et al., 2006). Human V6, like macaque V6, contains a complete retinotopic map of the contralateral hemifield (Pitzalis et al., 2006) and responds to coherent visual motion (Pitzalis et al., 2010, 2012, 2013a,b). So far, there is no conclusive evidence about the existence of a human homologue of macaque area V6A, although an extensive literature has shown activations in the posterior end of dorsomedial PPC, where V6A should be located, during arm reaching and pointing movements (e.g., Cavina-Pratesi et al., 2010; Filimon et al., 2007, 2009; Galati et al., 2011; Vesia et al., 2010). In our V6 study (Pitzalis et al., 2006), we revealed the existence of an additional retinotopic region anterior to V6 representing the periphery of the lower visual field, which

---

* Corresponding author at: Department of Education in Sport and Human Movement, University of Rome "Foro Italico", 00194 Rome, Italy. Fax: +39 06 36733 387.
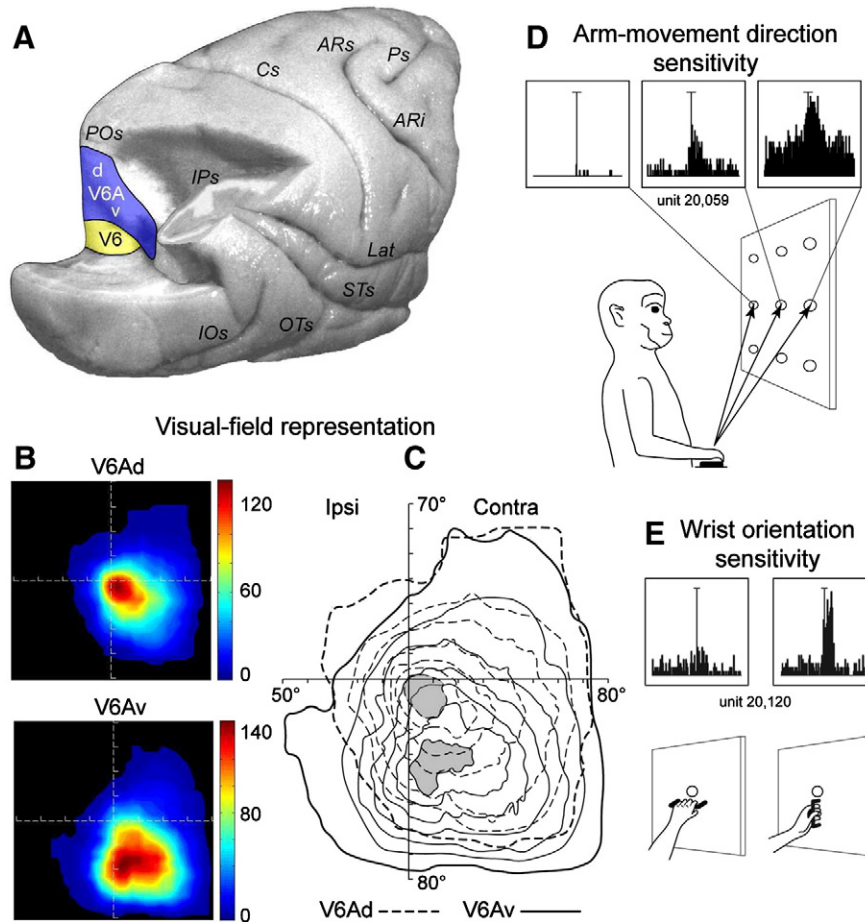E-mail address: sabrina.pitzalis@uniroma4.it (S. Pitzalis).

Fig. 1. Anatomical and functional definition of macaque V6A. (A) Anatomical position of area V6A in macaque brain (modified from Galletti et al., 1999b). The occipital pole and the inferior parietal lobule have been partially dissected to show the anterior bank of the parieto-occipital sulcus where V6A is located. (B) Visual field representation in V6Ad and V6Av, respectively (Gamberini et al., 2011). Colors from blue to red indicate the density of receptive field overlap. About one thousand of visual receptive fields were plotted in the figure. (C) Data shown in B are overlapped in C to better show similarities and differences between the two sectors of V6A (Gamberini et al., 2011). (D) Typical experimental set-up used on monkey to test V6A responsiveness to reaching movement, and response of a typical reaching neuron to different directions of arm movement (Fattori et al., 2005). (E) Monkey experimental set-up to test the modulating effect of wrist orientation, and response of a typical V6A neuron strongly modulated by the orientation of the wrist (Fattori et al., 2009a).

showed an inconsistent retinotopic organization. Here we systematically investigated the retinotopic and functional organization of this region using a combination of retinotopic mapping and functional MR. We showed that a region representing the contralateral lower visual field is systematically found anterior to human V6. This region, unlike V6, is also activated by hand and arm movements to visual targets, and we propose it as the human homologue of area V6A.

Material and methods

Subjects

A total of 12 experienced subjects participated in this study (9 women). The mean age was 31.3 years (ranging from 22 to 56). All participants, with normal or corrected to normal vision, gave their informed written consent prior to the scanning session, and all procedures were approved by the local Ethics and Human Subjects Committees. All 12 subjects participated in both the retinotopic and functional mapping experiments. Thus, each subject in total participated in 3–4 fMRI imaging sessions. Part of the retinotopic data used here has appeared previously (Pitzalis et al., 2006). Specifically, 3 out of 12 subjects were used also in Pitzalis et al. (2006) while 9 subjects were acquired ex novo. All subjects were right-handed, as assessed by a modified version of the Edinburgh Inventory (Oldfield, 1971) (mean index = 0.85; S.D. 0.15). Before scanning, subjects

were allowed, if they desired, to consume caffeinated beverages in order to better maintain alertness during the scan session.

Visual stimuli and experimental design

Retinotopic mapping

We mapped polar angle (measured from the contralateral horizontal meridian around the center of gaze) and eccentricity (distance from the center-of-gaze) using the same phase-encoded retinotopic stimuli previously used to map the visuotopic organization of human area V6 (Pitzalis et al., 2006). They consisted of high contrast light and dark colored checks flickering in counterphase in either a ray- or a ring-shaped configuration (polar angle and eccentricity, respectively). The average luminance of the stimuli was 105 cd/m^2. Each subject was presented with periodic stimuli (64 s/cycle, 8 cycles/scan), varying in eccentricity or polar angle. Stimuli moved slowly and continuously, and checks reversed between bright and dark at a rate of 8 Hz. Subjects viewed polar angle stimuli moving in both clockwise and counterclockwise directions in separate sessions. Stimuli were adjusted with respect to the distinctive characteristics of macaque V6 as described elsewhere (Pitzalis et al., 2006, 2010). We used (1) thin retinotopic stimuli (10° in polar angle), (2) a linear scaling in eccentricity (ring stimulus expanding at a constant speed of about 1°/s) and (3) a wide-field stimulation (up to 110° in total visual extent — see Experimental set-up). Finally, in some scans, the flickering checkerboards in the ring- and

ray-shaped apertures also contained superimposed white-dot optical flow fields, and streams (2–3 Hz, asynchronous) of eccentricity-scaled letters and faces. Subjects were required to fixate on the center cross while monitoring for occasional numbers (among the letters) and upside-down faces (among the right-side up). Compared with plain checkerboards, the additional visual shapes and tasks have been found to more consistently activate both lower and higher visual areas in humans (e.g., Pitzalis et al., 2006, 2010; Sereno et al., 2001).

Functional mapping

In the same group of subjects, we performed an additional experiment testing fMRI responsiveness to delayed finger pointing. In this study (hereafter called pointing), we used a blocked design with alternating periods of finger pointing and passive fixation in blocks of 16 s. The task was designed to maximally activate the reaching neurons of area V6A on the basis of the functional properties we observed in macaque neurons (see for review Gamberini et al., 2011), while taking into account the limitation of the fMRI method (artifacts created by large reaching movements). Thus, during the execution of pointing movements, subjects were requested to rotate their wrist in the target direction, which is a critical feature for activating V6A both in monkey (Fattori et al., 2009a) and human (Monaco et al., 2011).

At the beginning of the experiment, participants were required to maintain fixation on a white central fixation cross presented on a black background, and to use their right index to hold down a button of an MRI-compatible response box positioned centrally on their abdomen and attached to the scanner bed via Veltco straps. Each pointing block (Fig. 7A) started with the appearance of a written instruction at the center of the screen (POINT) and contained 4 trials in which subjects performed delayed pointing movements to the location of peripheral targets. At the beginning of each pointing trial, a peripheral target (a white circle of 0.9° diameter) was presented for 300 ms in one of 8 radial locations (1/8, 3/8, 5/8, 7/8, 9/8, 11/8, 13/8, 15/8 pi) at 4° of eccentricity. After a variable delay (1.5, 2.5, 3.5 or 4.5 s), the central fixation cross turned red for 300 ms, providing subjects the "go signal" to release the button and point with the right index to the remembered location of the peripheral target. Subjects were instructed to rotate their wrist to point the finger toward the target, while maintaining their eyes on the fixation cross, and without moving the shoulder or the arm; then, they were instructed to rapidly return their hand to the starting point and hold down the response key. The next trial started after 1 s. During fixation-only blocks, subjects were instructed by the initial written instruction (FIX) to maintain fixation throughout the block. Each scan contained 8 pointing blocks (duration: 16 s each) interleaved with fixation periods (duration: 13, 15.1, or 17.3 s). The onset of pointing movements was recorded in all sessions via a response box codifying button releases.

Experimental set-up

For the retinotopic mapping we used a wide-field stimulation, as that described in our previous paper (Pitzalis et al., 2006). Stimuli were projected onto a back-projection screen that was viewed directly (not via a mirror). The screen was placed only 10 to 12 cm from the subject so that visual stimuli subtended up to 100° (±50) horizontally, 80° (±40) vertically, and 110° (±55) in an oblique direction in the visual field. Besides better revealing areas that emphasize the periphery, the wide field retinotopic stimuli also help to deal with a critical confound in fMRI mapping studies due to surround inhibition (Brewer et al., 2002). As explained previously (Pitzalis et al., 2006, 2010; Sereno and Tootell, 2005), retinotopic cortical regions having representations of visual space just beyond the peripheral edge of a rotating wedge can generate a periodic signal with a misleading

180° phase offset. By stimulating most of the visual field, this beyond-the-stimulus-edge phase inversion is greatly reduced.

For the pointing study we used a standard field stimulation where the average viewing distance was 66.5 cm, and the screen size was 20 × 15°. Stimuli were back-projected onto a screen at the back of the MR bore that was visible to the subjects via a mirror. To measure fixation performance, horizontal and vertical gaze-positions were recorded with an infrared ASL eye-tracking system mounting long-range optics for use in the scanner and operating at 60 Hz (Applied Science Laboratories, Bedford, MA; Model 504). This system is fully MR-compatible and does not produce any artifact in the BOLD images. Fixation accuracy was quantified by calculating (in degrees of visual angle) the actual eye position with respect to the fixation cross. Fixation performance was measured only during a subset of fMRI retinotopic mapping and reaching experiments. Specifically, the ASL tracker was used only for the new data (9 subjects) that complemented the old datasets (3 subjects) taken from 2006. Also, useable data was not obtained with every subject for the usual reasons — e.g., difficulty maintaining pupil tracking across the experiment with light-eyed subjects and with an off-axis light path necessitated by larger visual field coverage. We obtained useable data only in six out of nine subjects, for which statistics are reported in the caption of Fig. 8. Head motion was minimized in most scans by using a bite bar with an individually molded dental impression mounted on a 6-degrees-of-freedom locking Plexiglas arm (Sereno et al., 2001). Subjects were instructed not to forcibly bite the impression but rather to use it as a reference. Subjects' heads were also stabilized with foam pads, and allowed to settle for a few minutes before the bite-bar arm was fixed in position. Interior surfaces were covered with black velvet to eliminate reflections. Stimuli were generated by control computers (a standard PC, an SGI O2, and a Mac OS X laptop, all equipped with 3D graphics cards) located outside the MR room and running software dedicated to each specific experiment. For the pointing study, stimuli were presented with an in-house software, implemented in MATLAB (The MathWorks Inc., Natick, MA, USA) using Cogent 2000 (developed at FIL and ICN, UCL, London, UK) and Cogent Graphics (developed by John Romaya at the LON, Wellcome Department of Imaging Neuroscience, UCL, London, UK). For the retinotopic mapping, stimuli were presented with an in-house OpenGL/Xlib program (Mapper software) coded by A. Dale and M. Sereno. Visual stimuli were projected using an XGA video projector (1024 × 768, 60 Hz, 10–15 pixels per degree of visual angle) whose standard lens had been replaced with a 7.38–12.3″ focal length XtraBright Zoom lens (Buhl Optical, USA) in order to achieve small high-resolution images on a screen inside the bore (at a distance of 3–4 m).

Imaging parameters

The MR examinations were conducted at the Santa Lucia Foundation (Rome, Italy) at 1.5 T (Siemens Vision, Siemens Medical Systems, Erlangen), 3 T (Siemens Allegra), and at the Birkbeck/UCL Neuroimaging Center (London, UK) at 1.5 T whole-body Tim Avanto System (Siemens Healthcare). Single-shot echo-planar imaging (EPI) images were collected using blood-oxygenation-level-dependent imaging (Kwong et al., 1992) by either a Small Flex quadrature surface RF coil placed over occipital and parietal areas (1.5 T Siemens Vision), a transmit–receive birdcage head coil (3 T), or a body transmit and 32-channel receive-only head coil (1.5 T Avanto).

For the retinotopic mapping, MR axial slices were 3.2 or 4 mm thick (with a 0 mm gap, interleaved excitation order), with an in-plane resolution of 3.2 × 3.2 mm or 3 × 3 mm, oriented approximately parallel to the calcarine fissure. Part of the retinotopic data were acquired with thinner slices (2.5 mm) and oriented approximately parallel to the calcarine fissure (thus covering all the brain). To increase signal to noise, data were averaged over four runs for

each stimulus type (eccentricity and polar angle). Thus in total, each participant underwent eight scans for the retinotopic mapping. Each scan took 512 s, with 260 single-shot EPI images (4 discarded).

For the functional mapping, the MR axial slices were 4 mm thick (with a 0 mm gap, interleaved excitation order), with an in-plane resolution of 3×3 mm, oriented approximately to the AC–PC line. From the superior convexity, sampling included almost all the cerebral cortex, excluding only the ventral portion of the cerebellum. Each participant underwent two scans of 256 s duration each. Other imaging parameters were as follows: 1.5 T Siemens Vision: 16–32 contiguous slices with time repetition (TR) = 2000 or 4000 ms, respectively; time echo (TE) = 42 ms, flip angle = 90°, 64×64 matrix, bandwidth = 926 Hz/pixel; 1.5 T Avanto: 24 contiguous slices, TR = 2000 ms; TE = 39 ms; flip angle = 90°, 64×64 matrix, bandwidth = 1474 Hz/pixel; and 3 T: 32 contiguous slices, TR = 2000 ms, TE = 30 ms, flip angle = 70°, 64×64 matrix, bandwidth = 2298 Hz/pixel. Overall, a total of 120 scans were carried out on the 12 subjects (96 scans to map retinotopic visual areas and 24 scans for the pointing experiment). In each scan, the first four volumes were discarded from data analysis in order to achieve a steady state, and the experimental tasks started at the beginning of the fifth volume. The cortical surface of each subject was reconstructed from a pair of structural scans (T1-weighted MPRAGE, $1 \times 1 \times 1$ mm; 1.5 T: 220 contiguous coronal slices, TI = 1000 ms, TR = 11.4 ms, TE = 4.4 ms, flip angle = 8°, or 176 contiguous sagittal slices, TI = 1000 ms, TR = 8.4 ms, TE = 3.6 ms, flip angle = 7°; 3 T: 176 contiguous sagittal slices, TI = 910 ms, TR = 2000 ms, TE = 4.38 ms, flip angle = 8°) taken in a separate session using a head coil. The last scan of each functional session was an alignment scan (also MPRAGE, $1 \times 1 \times 1$ or $1 \times 1 \times 2$ mm) acquired in the plane of the functional scans. The alignment scan was used to establish an initial registration of the functional data with the surface. Additional affine transformations that included a small amount of shear were then applied to the functional scans for each subject using blink in comparison with the structural images to achieve an exact overlay of the functional data onto each cortical surface.

Data analysis

Anatomical image processing

FreeSurfer was used for surface reconstruction (Dale et al., 1999; Fischl et al., 1999a). High resolution structural images obtained from each subject were manually registered and averaged. After reconstructing each hemisphere, we completely flattened the inflated occipital lobe after first cutting it off posterior to the Sylvian fissure, and making an additional cut along the calcarine fissure.

Analysis of retinotopic data

Retinotopic data were analyzed using FreeSurfer (Dale et al., 1999; Fischl et al., 1999a,b) based on standard procedures described in details in many previous studies (e.g., Hagler and Sereno, 2006; Pitzalis et al., 2006, 2010; Sereno et al., 1995; Tootell et al., 1997). Briefly, p-values were estimated on a voxel-by-voxel basis by constructing an F-ratio between 'signal' (response amplitude at stimulus frequency) and 'noise' (amplitude at other frequencies excluding 2nd and 3rd harmonics) with degrees of freedom equal to the number of time points. The phase of the signal at the stimulus frequency was used to map retinotopic coordinates (polar angle or eccentricity). In standard block-design analysis, pseudocolor scales are usually used to represent the amplitude of the response (after masking the data with a significance threshold). In mapping studies, pseudocolor is also used to represent the phase of the response. In order to concentrate the viewer's attention on the phase, we modulated the saturation of the color as a function of the signal amplitude using a sigmoid function. The sigmoid function was arranged so that visibly saturated phase colors begin to emerge from the gray background at a threshold of $p < 10^{-2}$. The data at most activated cortical surface

points has much higher significance values ($p < 10^{-5}$ to 10^{-10}). This procedure has been used in many previous studies (e.g., Tootell et al., 1997). A similar analysis was used to distinguish between positive and negative going MR fluctuations in the case of two-condition stimulus comparisons (e.g., MT + mapping). This analysis assumes that the noise is uncorrelated, an assumption known to be false for fMRI time series (Zarahn et al., 1997). Therefore the reported p-values should be considered rough estimates of the levels of statistical significance of the periodic activation. However, the lack of any trace of activation in large stretches of non-retinotopic visual areas in inferotemporal and inferior parietal cortices suggests that this threshold is not too permissive.

The boundaries of retinotopic cortical areas were defined on the cortical surface for each individual subject on the basis of phase-encoded retinotopy (DeYoe et al., 1994, 1996; Engel et al., 1994, 1997; Sereno et al., 1995) and subsequent calculation of visual field sign. This latter provides an objective means of drawing borders between areas based on the angle between the gradients (directions of fastest rate of change) in the polar angle and eccentricity with respect to cortical position (Sereno et al., 1994, 1995). The visual field sign indicates whether each small patch of cortex represents the visual field as a mirror-image or a non-mirror-image. As in non-human primates, early cortical areas (e.g., V1) are characterized by one visual field sign (e.g., mirror-image). Adjacent areas often have opposite visual field sign. Each field sign map shown here was based on 8 scans (4 scans for polar angle and 4 scans for eccentricity). The visual field sign method is merely a generalization of the notion that border between areas is often defined by meridians (but occasionally other lines in the visual field) with duplicated representations of visual space on either side of the meridian (or other line).

Here we used also the analysis of the phase movie to reveal the phase progression inside a specific cortical area. Although a series of color maps with superimposed isophase contour lines contains no more information than a single color map, the phase contours communicate the shape of the retinotopic map more precisely to the viewer than the colormap alone because small but significant variations in phase are hard to see with color hue alone (see e.g., Hadjikhani et al., 1998; Pitzalis et al., 2006). In particular, the phase contours more precisely illustrate the position of visual field meridians (maxima or minima of polar angle near −90, 0, and 90°), which are difficult to represent using hue alone. Such a series can also be thought of as the time sequence of activations for one stimulus cycle (though the width of the activated band of cortex at one point in time varies as a function of receptive field size and other factors). The phase of the periodic response is delayed because of a finite vascular response time. Also, it is possibly differently delayed in different areas. In our stimuli, the basic stimulus frequency was low enough so that the hemodynamic delay was much smaller than one cycle, eliminating whole-cycle phase ambiguity.

Data from a reversed-direction stimulus can be used to verify a map comparing the results obtained with opposite directions of movement within subjects. Test 1 responses can therefore be used to predict test 2 responses with one free parameter, the hemodynamic delay (which is, however, small relative to the time for a full cycle of stimulus rotation). To make it easier to compare the results with those obtained in test 1, we reversed the color map and added half a cycle of phase angle, so that upper, middle, and lower fields are colored the same for both directions of rotation.

Reversed data can also be combined with unreversed data to correct residual phase delay differences between areas (Hagler and Sereno, 2006; Sereno et al., 1995). We calculated the vector average at each voxel of the response amplitude and phase angle obtained for opposite directions of stimulus motion (clockwise versus counterclockwise) after reversing the sign of the phase angle for one direction. This procedure reduced noise in both visual and non-visual cortical areas because the vector sum operation strongly penalizes

voxels with inconsistent phase in opposite directions, even if they are separately significant.

To average retinotopic mapping data across subjects, we used a method for group analysis of phase-encoded retinotopic mapping data developed by our group (Hagler and Sereno, 2006). The individual unfolded cortical surfaces were first inflated to a sphere, and then nonlinearly morphed into alignment with a canonical target sphere brain (icosahedral supertessellation) by minimizing local differences in average convexity ["sulcusness" (Fischl et al., 1999b, their Eq. 9)] while also minimizing metric distortion (FreeSurfer5.0, MGH NMR Center). Complex-valued single-subject mapping data (amplitude and phase of significant periodic responses), were averaged across subjects by vector addition at each vertex of the canonical spherical surface. As with vector averaging of clockwise–counterclockwise data, this procedure strongly penalizes surface locations with inconsistent phase across subjects, even if those locations are significantly activated in each subject. The average map was then resampled back onto the fsaverage surface (FreeSurfer 5.0) for display and thresholded using a complex F-statistic (Hagler et al., 2007). This averaging procedure was justified by the fact that surface-based morphing does a good job of aligning independently obtained retinotopic maps (Fischl et al., 1999b). Data were then sampled back to an individual brain via the common icosahedral coordinate system.

Definition of retinotopic ROIs

The phase of the fitted response was taken as an index of visual field location, in terms of polar angle. Reversals of the direction of phase change across the cortical surface were taken as boundaries of visual areas (Sereno et al., 1995). Retinotopic ROIs (visual areas V3A, V6 and V6A) were drawn on the basis of these boundaries viewed on a flattened version of each participant's reference anatomy.

In order to provide stereotaxic coordinates we projected back each individual ROI into volume space and then to standard ICBM152 space, using a nonlinear transformation whose parameters were estimated from each subject's structural image using the stereotaxic normalization algorithms provided by the SPM8 software (Wellcome Department of Cognitive Neurology, London, UK). Average coordinates of each region were determined on the basis of the center of gravity of each individual ROI in ICBM152 space.

For display purposes, individual retinotopic ROIs were projected onto the CONTE69 atlas surface (Van Essen et al., 2012) and combined across subjects to display probabilistic maps of each ROI, where the value at each surface node of the CONTE69 atlas represented the proportion of subjects whose ROI included that node.

Analysis of functional data

Functional images from the pointing experiment were preprocessed and analyzed using SPM8. Functional time series from each subject and scan was realigned within and across scans to correct for head movement and coregistered with structural MPRAGE scans, and thus to the reconstructed surface. Functional data from each individual were then projected to his/her surface space by assigning to each surface vertex the BOLD time course of the voxel within which that vertex was located. These time courses were then averaged across the vertices within each individual retinotopic ROI, to build a reference BOLD time signal for each surface-based retinotopic ROI. These reference time courses were analyzed according to the general linear model (GLM). Hemodynamic responses associated with pointing blocks were modeled as a box-car function convolved with an idealized representation of the hemodynamic response function, as implemented in SPM. Passive fixation blocks were not explicitly modeled as GLM regressors and thus treated as part of residual variance. A parameter estimate was obtained for each retinotopic ROI in each individual hemisphere, that represented the estimated percent signal change during pointing blocks relative to baseline. Parameter estimates in retinotopic regions were then compared using a random-effects analysis in which the hemisphere was treated as a random effect.

Results

Retinotopic mapping

Polar angle representation

In Fig. 2 the inflated (A) and the flat (B) representations of the posterior portion of the left hemisphere of a representative subject indicate the typical position of the POs on the medial wall with respect to the calcarine sulcus and the pIPS (see caption for details). The left column of Fig. 2C shows the CCW polar angle maps in the left hemisphere of two subjects. Here the periphery was stimulated most completely — up to 110° total visual angle. As previously reported (Pitzalis et al., 2006) human V6 (yellow outline), like macaque V6, represents retinotopically the entire contralateral hemifield, with upper fields located medial to areas V2/V3, and lower fields medial to areas V3/V3A. Moving in the figure to the left of V6 (anteriorly in the brain) the presence of an additional lower field representation (dotted white outline) is evident in both subjects. This retinotopic region, which does not appear when standard-size mapping stimuli are used, was systematically located on the dorsalmost part of the POs, anterior to the lower-field representation of V6 and medial (up in the figure) to the peripheral lower field representation of area V3A.

Since this lower field representation adjoins the lower representation of V6, the analysis of the phase progression inside the area was essential to exclude that it was actually part of V6 (see Material and methods for details). The analysis of the phase movie (Fig. 2D) revealed that much of the green spot bordering anteriorly area V6 (to the left of it in the figure) does not belong to area V6. Indeed the phase contour splits and moves apart in the middle of the green spot (see white arrows pointing to the phase reversal in Fig. 2D, third snapshot of both subjects) indicating the presence of a vertical meridian and thus the presence of a second, more dorsal representation of the lower visual field outside and anterolateral to that seen in V6. Specifically, this lower-field-only representation was separated from the more posteriorly located lower field in V6 by an intervening vertical meridian (100% of cases). The lateral border of this region was defined by a horizontal meridian (85% of cases) that bordered areas V3A and/or V7. Contralateral versus ipsilateral contrasts in voxels from this newly defined region revealed that contralateral targets were strongly preferred ($p = 10^{-4}$ to 10^{-9}). The analysis of the phase progression inside the new area was essential to distinguish it as another lower visual field representation alongside the one in neighboring area V3A. Tootell et al. (1997) used smaller visual stimuli that stimulated less of the periphery; this likely made it difficult for them to distinguish this additional reversal (see white arrow in frame 3 of Fig. 2D).

To verify the reliability of the retinotopic organization of the lower-field-only area, we reversed the direction of rotation of the polar angle stimulus and compared the results obtained with opposite directions of movement within subjects (see Material and methods for details). The right column of the right column of Fig. 2C shows the results of the reversed (CW) stimulation on the left hemispheres of the same two subjects. Results show that the position of the newly-defined lower-field-only area with respect to the POS and other visual areas is nearly constant across subjects, hemispheres, and sessions. Direct comparison between the opposite-rotation-derived lower-field-only maps (anterior to V6) shows that they were nearly identical in these two subjects, even though they were acquired in independent experiments, performed months apart and with a reversed direction of rotation.

Moving anteriorly to this lower-field-only area, we found that the retinotopy was less consistent across subjects (e.g., the retinotopy in this region is quite different in the left and right hemispheres — data not shown) and also across sessions from the same subject (see subj. 2, in Fig. 2C). Upper visual fields were found in a minority of subjects (30%). If present, upper fields were variably located either
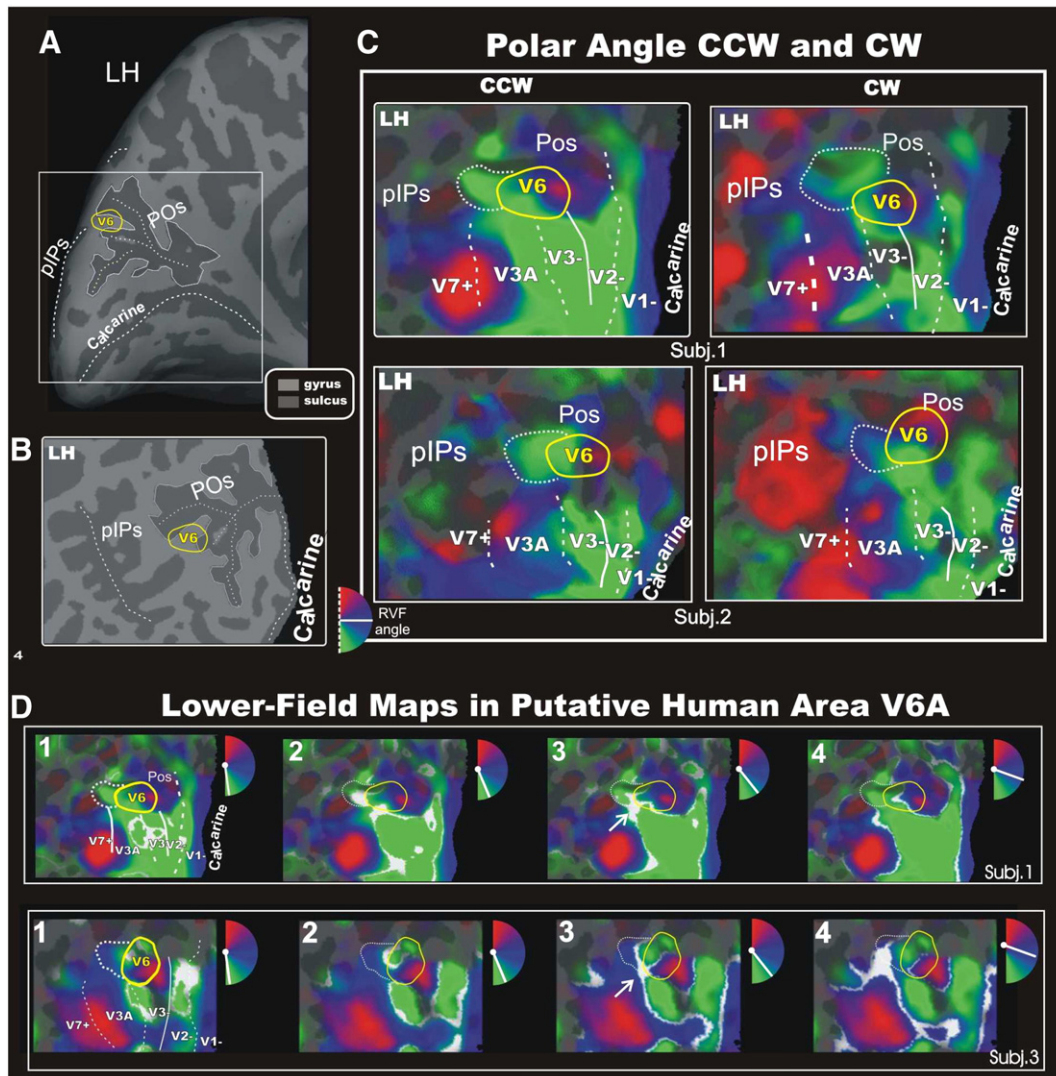
Fig. 2. Polar angle maps in putative human area V6A (CCW and CW). (A) Inflated representation of the posterior portion of the left hemisphere of a representative subject indicating the position of the POs on the medial wall respect to the calcarine sulcus and the pIPS. The cortical surfaces were defined at the gray-white matter border and have been inflated to reveal regions within the sulci (concavities, dark gray) as well as on the gyri (convexities, light gray). (B) Flat representation of the portion of the inflated brain inside the white box showing for reference the corresponding positions of these three sulci (Pos, pIPS and calcarine) on the flat map. The same part of the brain shown in the flat map (B) is shown in the close-up images rendered in C and D and next Fig. 3–4. In A and B the key sulci are indicated by dashed white lines. (C) CCW (left) and CW (right) polar angle maps displayed on close-ups of the flattened cortical surface representation from the left (LH) hemisphere of two participants. Color hue indicates the response phase, which is proportional to the polar angle of the local visual field representation. Red, blue, and green areas represent preference for upper, middle, and lower parts of the contralateral visual field, respectively. The map color scheme for clockwise runs is reversed to make it consistent with counterclockwise runs. (D) The eight panels show close-up maps of polar angle in V6A in the left hemispheres of two subjects. In each frame, a response-phase contour is marked with a white stripe and half range of phases in one lower hemifield (90°) is illustrated across the four close-ups of the flattened surface. The white areas on each panel represent the cortical regions activated by a single polar angle, indicated in white in the small hemifield icons located at the upper right of each snapshot. In all sections, yellow outlines indicate location and borders of the human area V6 (Pitzalis et al., 2006). In all close-ups (C–D), only the dorsal stream is shown together with the borders of the dorsal visual areas identified in these subjects by retinotopic mapping (V1−, V2−, V3, V3A, V7; Sereno et al., 1995). On the flat map, dotted and solid white lines indicate vertical and horizontal meridians. POs, parieto-occipital sulcus, pIPS, posterior end of the intraparietal sulcus.

on the POS or on the posterior end of the IPS (labeled pIPS in the figures). In the latter case, it was sometimes not clearly separated from the upper field of V3A (suggesting it might belong to it; see subj. 2-CW) while in other cases it was separated from the upper field of V3A by a horizontal meridian (see subj. 1-CCW). Consistency is one of the main criteria to assign reliability to a newly defined retinotopic region and this variable upper field region is not consistent. Hence we concentrated our analysis on the lower-field-only region. For ease of comparison this region will be hereafter called area V6A.

Although data from a reversed-direction stimulus can be used to verify a map, reversed data can also be combined with unreversed data to correct residual phase delay differences (Sereno et al., 1995). We applied this procedure to our data. Fig. 3 shows the wide-field polar angle maps in four (subjects 3–8) additional participants (eight hemispheres). In this case, two CCW and two CW polar angle scans for each subject were combined to cancel hemodynamic delay differences among areas. A small strictly contralateral representation of the V6A lower-field (dotted white outline) was visible in all 8 unfolded hemispheres in medial (rotated to posterior) view, located anterior to the lower-field representation of V6 (yellow outline) and separated from the more posterior lower field in V6 by intervening vertical meridian. The similarity of these images to ones obtained with unidirectional data (Fig. 2) confirms that delay differences between areas were small relative to the full cycle time.

We also performed a surface-based group analysis of phase-encoded polar angle data (for details, see Material and methods). Average results are shown in Fig. 4. The position and borders of the new region are indicated with a dotted white outline. The location and retinotopic
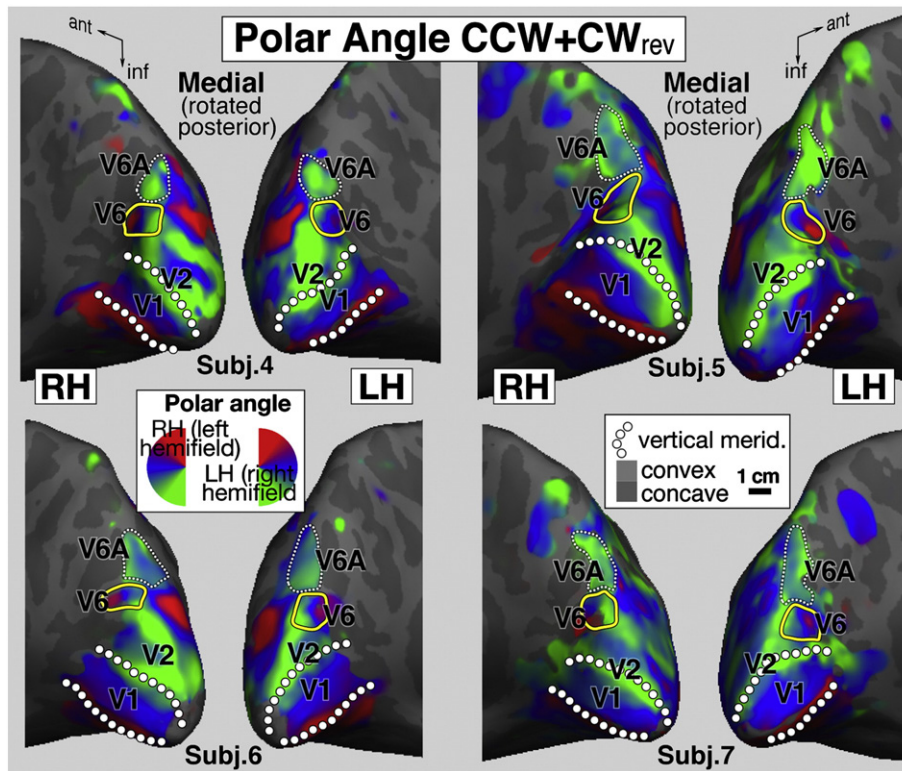
Fig. 3. Polar angle maps in putative human area V6A (CCW + CWrev). Results from both hemispheres [left hemisphere (LH); right hemisphere (RH)] of four additional participants are shown in medial (rotated to posterior) inflated views. In this case, two CCW and two CW polar angle scans for each subject were combined (by reversing the response phase of the CW scan and taking the voxel-wise vector average of all 4 scans) to cancel hemodynamic delay differences among areas. Other labels and conventions are as in Fig. 2.

organization of the new area were confirmed in the average map. Indeed the lower-field-only representation was located on the dorsalmost part of the POs, anterior to the lower-field representation of V6 (yellow outline) and medial to the peripheral lower field representation of area V3A. This lower-field-only representation was separated from the more posterior lower field in V6 by an intervening vertical meridian. The general organization of the V6A average maps closely parallels the individual data (Figs. 2–3). Note that the statistical procedure used for the average data reduces noise in both visual and non-visual cortical areas because the vector sum operation strongly penalizes voxels with inconsistent phase across subjects. In this analysis, the variable upper field activation sometimes found anteriorly to V6A described before not unexpectedly disappeared. But the V6A and the V6 maps were found in exactly the same position showing that delay differences between subjects were small. The dorsal red spot observed in some cases was not consistent in the same way as V6 and V6A and that is why we did not include it in the map.

Overall, the individual and group analyses of the polar angle data demonstrate the presence of an additional area in the dorsal stream with a systematic representation of the contralateral lower visual field that is separated from the lower field in V6 by a vertical meridian (see doubling of phase contour in Fig. 2D). The polar angle representation of this new region is similar to that observed in the macaque V6A, where Galletti et al. (1996, 1999b) described a clear over-representation of the contralateral lower visual field adjoining anteriorly the lower visual field of V6.

Eccentricity representation

Fig. 5A shows several individual eccentricity maps. To aid comparisons, the dotted outline of the V6A of each subject, as obtained by polar angle mapping, has been drawn on the maps, together with the vertical and horizontal meridian representations of early visual areas and the outline of area V6 (in yellow; see captions for details).

Unlike V6, V6A lacks of a representation of the center of gaze in all subjects, although it shows a small trend in eccentricity (see below).
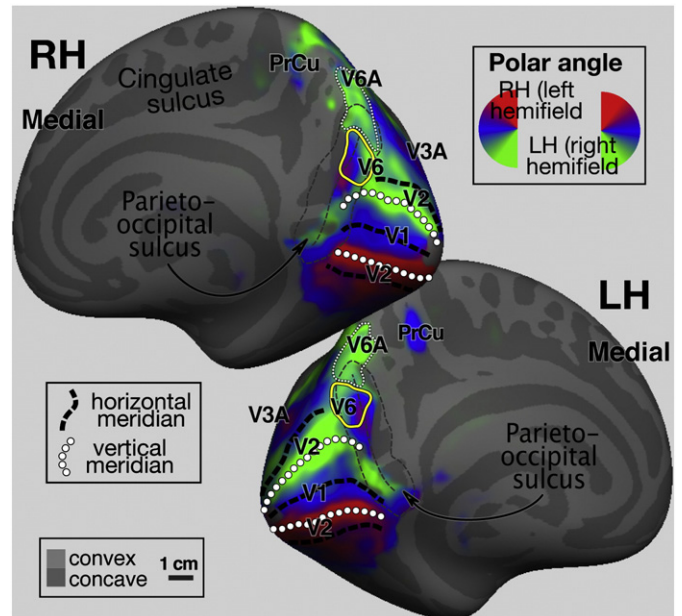

Fig. 4. Average polar angle maps rendered on the inflated left (LH) and right (RH) hemispheres of the FreeSurfer 'fsaverage' surface (rotated toward posterior view as in Fig. 3). CCW and CW polar angle scans were combined in each subject to cancel hemodynamic delay differences among areas and then vector-averaged across subjects using sulcus-based surface morphing. The yellow borders indicate the position of human area V6. The dotted borders indicate V6A, an extra lower-field representation anterior and superior to V6. Horizontal and vertical meridians of average retinotopy in early visual areas are indicated by thick dashes and lines of small circles (PrCu, precuneus; other labels as in Fig. 2).

The pseudo-color scale shows that the cortical region inside the dotted outline is entirely green (no blue voxels representing intermediate periphery is present). This means that the area contains only a peripheral representation ($> = 30°$) and lacks the central part of the visual field (80% of the cases). The analysis of the eccentricity phase movies (Fig. 5B) shows that V6A started to respond to visual stimulations only at 30° of eccentricity (panels 1–2). Activation then moved inferiorly within V6A, on the inflated mesial surface, in a dorso-ventral direction (upward and rightward in panels 3–4 of Fig. 5B). This means that the more central representation of the area is located dorso-laterally and the most peripheral part ventro-medially, close to the peripheral representation of V6 (where the phase moves in opposite directions).

In 60% of the cases, we observed that V6A continues to respond to the most peripheral stimulations when area V6 is nearly switched off (see panel 4 in Fig. 5B). In other words, V6A responds to a greater portion of periphery than even area V6. In addition, the phase movies show that in most cases (80%) the phase in area V6A moves in opposite directions to that in areas V6 and V3A. In summary, we believe that the polar angle and eccentricity data, together with observations on visual field duplication argue that V6A is a new independent lower field representation.

Fig. 6 shows a map of the visual field sign (yellow, mirror image of visual field; blue, non-mirror image of visual field) on the flattened surface of the left and right hemispheres of two participants, calculated from the maps of polar angle and eccentricity from the same subjects, as described previously (Sereno et al., 1995). The area we have defined as human V6A contains a non-mirror-image representation. It is located anterior to the mirror-V6 and just above the non-mirror V3A, and is present bilaterally in all subjects.

Retinotopic ROIs

From the analysis of phase-encoded polar angle data, we drew three retinotopically defined regions of interest (ROIs) in each subject: V3A, V6 and V6A (see Material and methods). The ROI definitions were as follows. V3A was defined as a complete representation of the contralateral visual field anterior to dorsal V3, in correspondence of the posterior segment of the intraparietal sulcus (pIPs) (Tootell et al., 1997). V6 was defined as a complete representation of the contralateral visual field located on the posterior bank of the dorsalmost portion of POs. The borders of human V6 were defined by 2 vertical meridians, a medial one superior and anterior to peripheral lower field V2/V3 and a lateral one
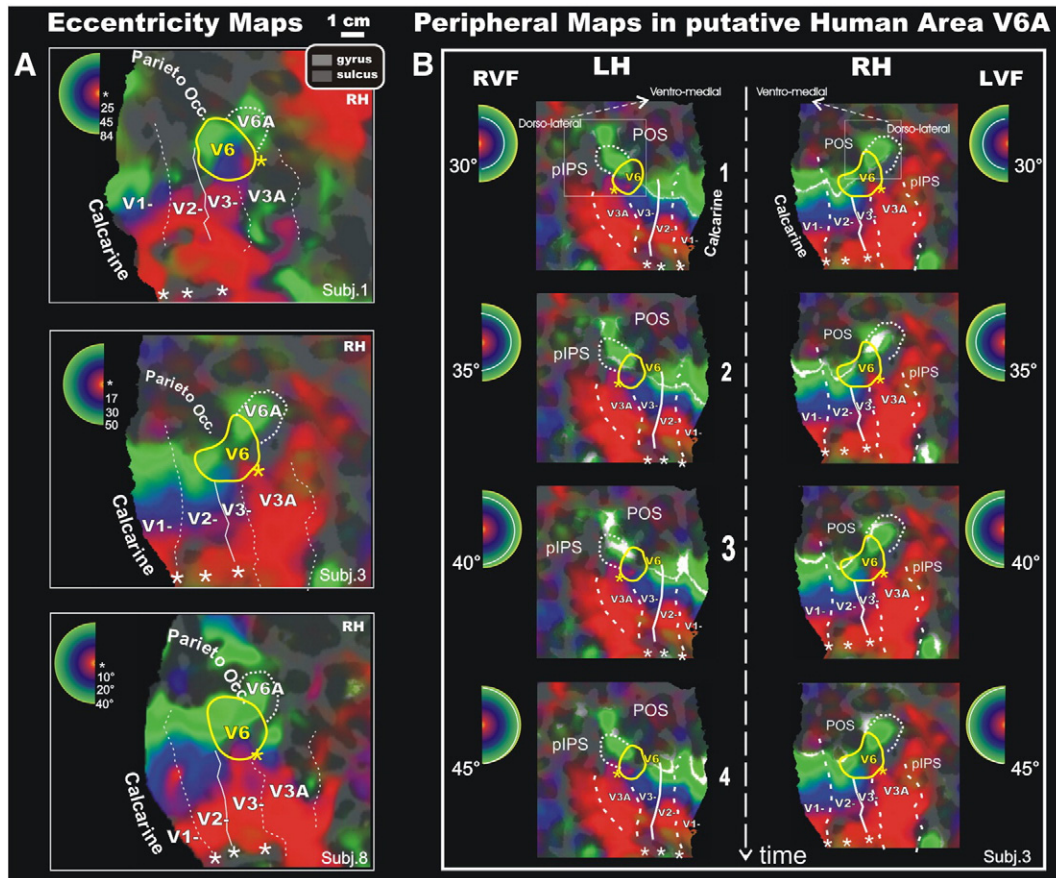

Fig. 5. Phase-encoded eccentricity maps in putative human area V6A. (A) Figure shows color plots of the response to a wide-field ring stimulus expanding at a constant slow speed (about 1°/s), displayed on close-ups of the right (RH) flattened cortical surface of three participants (only the dorsal visual stream is shown). The representation of central-through-more-peripheral eccentricities is coded using red-blue-green, respectively (see inset, located at the upper left of each snapshot). The hue of the color at each cortical surface point again indicates the response phase, but now it is proportional to the eccentricity of the local visual field representation. Each inset indicates the maximal periphery we were able to reach in that subject. To aid comparisons, the dotted outline of putative area V6A of each subject, as obtained by polar angle mapping, has been drawn on the eccentricity maps together with boundaries of dorsal visual areas V1, V2, V3, V3A and V6. The representations of the center of gaze are indicated with asterisks (other labels as in Fig. 2). Unlike V6, putative area V6A lacks a representation of the center of gaze. (B) The eight panels show a close-up map of the detailed organization of the eccentricity representation within area V6A (in white box in the first snapshots) as a temporal sequence of activation in the left (LH; first column) and right (RH; second column) hemispheres of one subject (subj. 3). Only the peripheral 30° to 50° of eccentricity is shown in four steps in the direction indicated by the dashed white arrow. The white bands on each panel represent the cortical regions activated by progressively more peripheral eccentricities and show that V6A only starts to respond from 30° onward. Eccentricity increases moving inferiorly, as indicated by the dashed arrows in the first frame of the LH and RH. RVF, right visual field; LVF, left visual field.
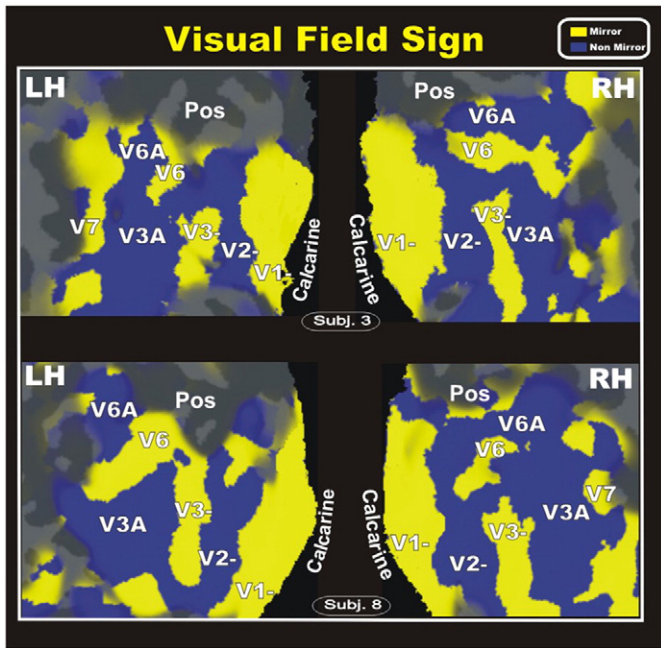
Fig. 6. Maps of retinotopic field sign in area V6A. Analysis of retinotopic data (polar angle and eccentricity) by visual field sign (mirror-image versus non-mirror-image visual field representation) (Sereno et al., 1995). Mirror-image areas (yellow; e.g., V1), and non-mirror-image areas (blue; e.g., V2) are shown in the left (LH) and right (RH) flattened hemispheres of two participants. The lower field representations of V1, V2, V3, V3A, V6 and V7 (if any) are labeled, along with V6A. Note that V6A contains a non-mirror-image representation, like V2 and V3A, and opposite to V1 and V3.

superior to V3A (Pitzalis et al., 2006). V6A was defined as the lower-field-only region located just anterior to V6, on the anterior bank of the POs, medially to V3A. Each of the three ROIs was drawn on both hemispheres of all subjects (N = 12), for a total of 72 retinotopic ROIs (see Fig. 7, left and right columns).

Fig. 7 shows also superposition of the individual retinotopic ROIs (N = 72) in standard ICBM152 space, projected onto the left and right hemispheres of the CONTE69 atlas surface (Van Essen et al., 2012). In Fig. 7 the three types of ROIs are color coded (V6A, blue; V6, yellow; V3A, red) and are superimposed on a semi-inflated (top), folded (middle) and flattened (bottom) view of the CONTE69 atlas surface (Van Essen et al., 2012). On the flat maps, the fundus (dashed lines) of the POs and pIPs is drawn to aid the anatomical location of area V6A with respect to the sulcal anatomy and the neighboring areas V3A and V6.

As in macaque, human V6A (blue) is reliably located in or near the anterior bank of the dorsal end of POs. The average coordinates of area V6A (as defined retinotopically in this study) in ICBM152 space were x = ±15.5, y = −75.8, and z = 38.6.

As previously demonstrated (Pitzalis et al., 2006), the retinotopic map of V6 (yellow) is consistently located in or near the posterior wall of the POs, corresponding to the following average ICBM152 coordinates (x = ±14.2, y = −81.6, z = 32.5).

Note in Fig. 7 the position of areas V6 and V6A within the dorsal end of POs: although the two areas are somewhat dispersed around the upper part of POs, they are segregated within the posterior and anterior walls of the POS, respectively. The most dorsal part of the human POs often has a "Y" shape, with anterior and posterior branches variably configured across individuals. When this is the case, areas V6 and V6A lie in the posterior and anterior branches of the POs (Pitzalis et al., 2006), respectively.

Area V3A (red) is located on the posterior segment of the intraparietal sulcus (pIPs) corresponding to the following average ICBM152 coordinates (x = ±24.8, y = −84.3, z = 23) which fit well with the coordinates found by Tootell et al. (1997).

Functional profile of retinotopic ROIs

Macaque monkey area V6A is not only defined by its anatomical location and retinotopic properties (i.e. a region in the anterior bank of the POS that over-represents the contralateral lower field, with particular emphasis on the far periphery), but also by its responsiveness to spatially-directed reaching movements (Fig. 1D; see Galletti et al., 2003 for review). The adjacent area V6, a strictly visual extrastriate area, is, by contrast, unresponsive during reaching movements in darkness (see Gamberini et al., 2011 for review).

Therefore, to bolster the notion of a homology between the monkey area V6A and the human V6A described here, we examined the magnitude of the evoked responses in V6 and V6A to pointing movements that required the subject to rotate the wrist, a critical feature for activating V6A both in monkey (Fattori et al., 2009a) and human (Monaco et al., 2011). The pointing experiment was conducted on the same 12 subjects already tested in the retinotopic mapping (but 2 subjects were excluded from the analyses because of excessive head movements during the scans).

Based on previous work on monkey areas V6A and V6 and human area V6 (Fattori et al., 2001, 2005, 2009a,b; Galletti et al., 2003; Pitzalis et al., 2010), we expected greater responses to pointing movements in area V6A relative to areas V6. To test this prediction, we compared the response (the BOLD percent signal change extracted from each hemisphere) of these two regions to pointing execution.

Fig. 8B illustrates the mean and standard error of the BOLD percent signal change associated with pointing movements in each region. Pointing responses were very strong in V6A and non-existent in V6, and a paired t-test indicated that the difference between the BOLD responses of these two regions to pointing movements was statistically significant ($T_{19} = 6.6$, $p < 0.001$).

Fig. 8C shows the estimated percent BOLD signal change for each individual hemisphere in V6 and V6A during pointing. Individual data show that V6A was positively activated in all hemispheres during pointing, while no consistent signal was observed in V6. All but one of the points are located above the main diagonal, implying more activation in V6A than in V6 for almost every hemisphere.

In conclusion, we found that area V6, as defined by retinotopy, was not activated during pointing, whereas the additional lower visual field region adjoining V6 anteriorly was strongly activated during pointing movements. This indicates that this new region – putative human V6A – is functionally independent from human V6.

Comparison with macaque data

In order to provide definitive evidence that the lower-field-only representation that we found at the border of the human V6 actually corresponds to the human homologue of macaque area V6A, we re-analyzed the large amount of monkey data that has been collected in our laboratory. Monkey data came from 7 animals (*Macaca fascicularis*) studied in over fifteen years. In these animals, extracellular recordings allowed us to characterize the functional properties of more than one thousand cells in V6A. The recording site of each of these cells was reconstructed on the brain of single cases by applying the methodology described in Galletti et al. (1996). Single cases were then combined on an atlas brain using CARET resources (Van Essen, 2005; see Gamberini et al., 2011).

Fig. 9 shows the results. In Fig. 9B the anterior bank of the parieto-occipital sulcus is fully visible after cutting away the portion of the occipital pole indicated in Fig. 9A. Fig. 9B shows the limits of area V6A (continuous line), as well as the locations of the nearby areas V6 and PEc, and the separation of area V6A into dorsal (V6Ad) and ventral (V6Av) subdivisions (dashed line) on the anterior bank of POs. These subdivisions and areal borders come from a detailed analysis of the cytoarchitecture of this portion of the cerebral cortex (Luppino et al., 2005).
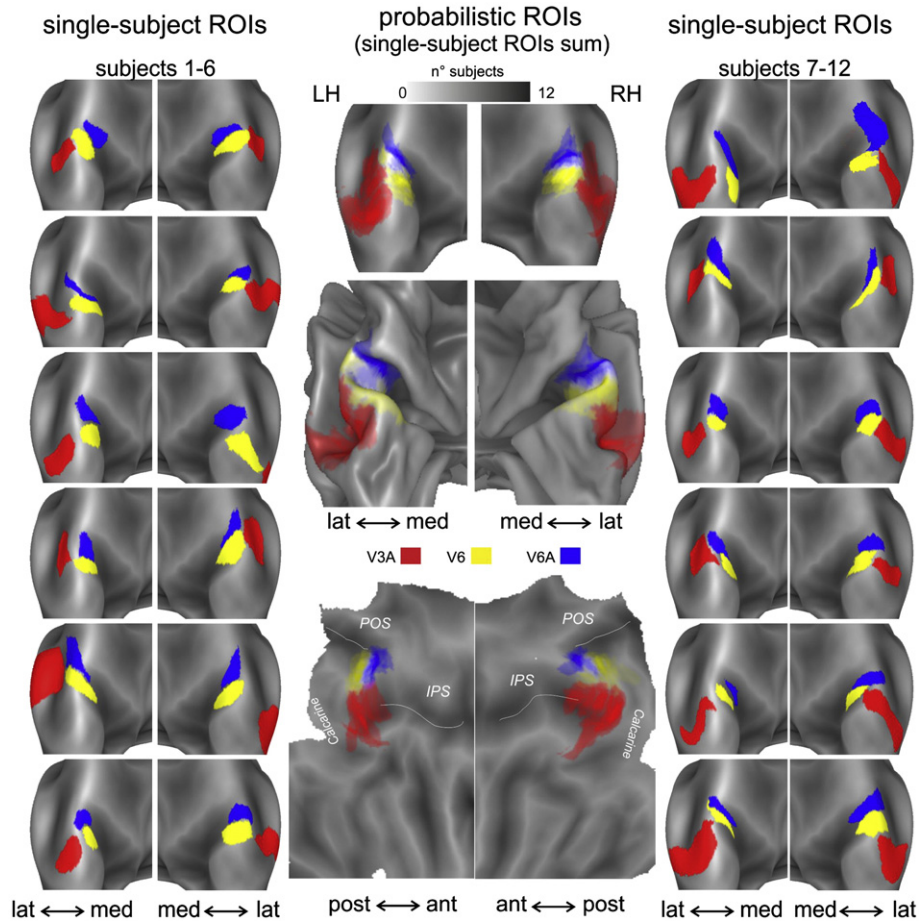
Fig. 7. Brain location of retinotopic ROIs. Left and right columns: 72 individual ROIs (3 ROIs × 2 hemispheres × 12 subjects) are displayed on a close-up of the parieto-occipital sulcus of the CONTE69 atlas surface (Van Essen et al., 2012). V3A is shown in red color, V6 in yellow and V6A in blue. Middle column: The sum of individual V6, V6A and V3A ROIs is also superimposed over an inflated (top), folded (middle) and flattened (bottom) view of the same atlas surface. The color scale indicates overlap of individual ROIs in each surface node. On the flat maps, the fundus of the parieto-occipital sulcus (POs) and the posterior end of the intraparietal sulcus (pIPs) are marked by dashed white lines.

In Fig. 9C, we show the distribution, within area V6A, of the visual cells sensitive to simple visual stimuli, such as light/dark borders and bars ("low-level" in Fig. 8C) moved across the neuron's receptive fields, and to complex visual stimuli, such as hand shadows continuously moving and changing in shape ("high-level" in Fig. 9C). Note that the responses to optimal moving stimuli of low-level cells were typically much stronger than those of the high-level cells, and most high-level cells were unresponsive to simple visual stimuli. From Fig. 9C and Table 1 it is evident that the low-level cells were concentrated in the

ventral part of V6A (69% low-level cells vs. 31% high-level cells), whereas the high-level cells were almost equally represented in the two sectors of V6A.

Fig. 9D shows the distribution of low-level visual cells with receptive fields located in the central 30° of the visual field, and in more peripheral regions ($>= 30°$). It is clear that V6Av contained many more cells with peripheral than central receptive fields (76% vs. 24%; Table 1). In contrast, central and peripheral cells were present in V6Ad with about the same incidence.
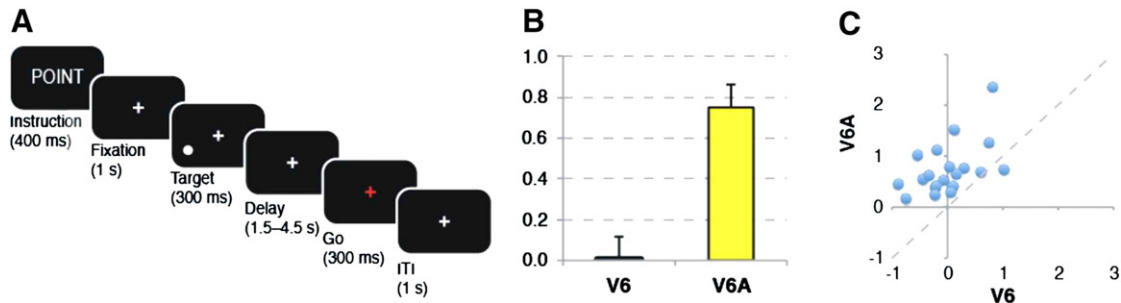

Fig. 8. Functional mapping. (A) Visual stimuli and sequence of events during the pointing blocks. Subjects start fixating a central white cross (fixation). After 1 s a peripheral white circle is presented for 300 ms (target). After a variable delay, when the central fixation cross turns red (go) the subjects point with the right index to the remembered location of the peripheral target, while maintaining fixation. They then immediately move back to the starting position and the following trial starts after 1 s (ITI). The fixation stability of a subset of expert subjects (6 out of 9), for which reliable eye data were recorded (see Material and methods), was excellent (S.D. = 0.7° for the retinotopic mapping and S.D. = 0.95° for the pointing task) and in line with standard parameters (e.g., Crossland et al., 2008; Di Russo et al., 2003; Fischer et al., 2012). (B) Mean BOLD percent signal change during pointing blocks in each ROI. (C) Individual results for pointing blocks in areas V6 and V6A.
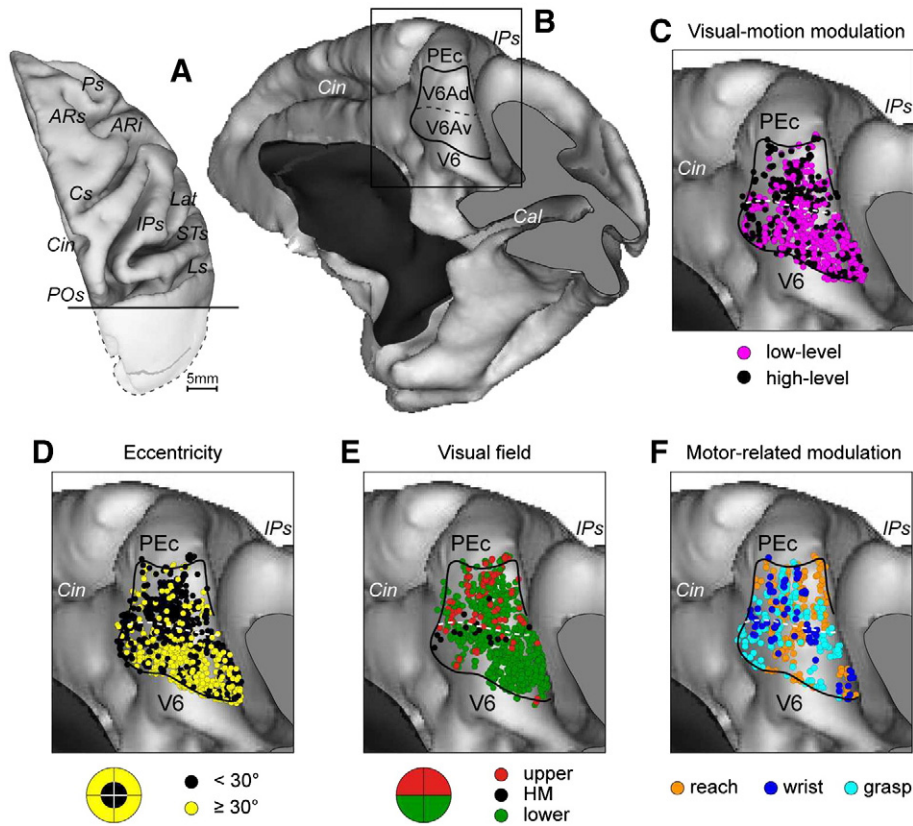
Fig. 9. (A) Distribution of functional properties in macaque area V6A. (B) Postero-medial views of a macaque right hemisphere showing the locations of area V6A, of its dorsal and ventral sectors (V6Ad and V6Av, respectively), and of the nearby areas V6 and PEc. The occipital pole was cut away, as indicated in the dorsal view of the hemisphere in A, to show the anterior bank of the parieto-occipital sulcus where the cortical areas are located. (C) Distribution of low- and high-level visual cells in areas V6Ad and V6Av. (D) Distribution of low-level visual cells with receptive fields in the central (<30°) and peripheral (>30°) visual fields, respectively. (E) Distribution of low-level visual cells with receptive fields in the lower or upper visual field, or centered on the horizontal meridian. (F) Distribution of cells sensitive to reaching arm movement, to wrist orientation, or to the type of grip used to grasp an object.

Fig. 9E shows the distribution of visual cells with receptive field in the upper or lower visual field. It is clear (see also Table 1) that V6Av was dominated by cells representing the lower visual field (90% lower vs 8% upper). The prevalence of lower field representation was also evident in V6Ad (73% vs. 20%). It is worth noting that the cells with receptive field centered on the horizontal meridian were located along the border between V6Av and V6Ad.

Fig. 9F shows the distribution within V6A of cells whose activity was modulated by reach-to-grasp movements. We distinguish cells modulated by reaching arm movements, by wrist orientation, and by grip type during grasping (Fattori et al., 2001, 2005, 2009a, 2010). All three types of cells were well represented in both subdivisions of area V6A.

Discussion

Human V6A: a retinotopic area for reaching

In the first part of this study, we mapped the retinotopic organization of human visual area V6A using wide field stimulation. In all subjects, we found a retinotopic map of the contralateral lower visual field in the most superior part of the anterior bank of the parieto-occipital sulcus. It was anterior to the map in V6, joining it at a lower vertical meridian, and just anterior and medial to peripheral V3A/V7 lower representations. In contrast to human V6, human V6A lacks a representation of the center of gaze; it responds only to visual stimulation of the far periphery (starting from 30°). Analysis of eccentricity data shows that there is a tendency for eccentricity to increase as one moves inferiorly and posteriorly. Visual field sign

calculations show that V6A has a non-mirror-image representation, like V2 and V3A but opposite to V6. The macaque receptive field data is consistent with this. Like macaque V6A, human V6A has an over-representation of the lower visual field as well as of the periphery (Galletti et al., 1996, 1999b).

In the second part of this study, we sought to find out whether human V6A has the same functional properties as macaque V6A. Unlike V6, monkey V6A is known to contain arm-movement-related cells (Fattori et al., 2001) and to be responsive to spatially-directed reaching movements (Fattori et al., 2005) as well as changes in wrist orientation (Fattori et al., 2009a). A second fMRI experiment tested whether the human V6A showed consistent BOLD responses to finger pointing movements that required changes in wrist

Table 1
Distribution of cell types in macaque area V6A. Columns report the number (and percentage) of different types of cells in the two sectors of area V6A (V6Av and V6Ad). First and second rows: low-level- and high-level cells are cells activated by simple and complex stimuli, respectively (see Material and methods). Third and fourth rows: cells with visual receptive fields centrally (<30° eccentricity) or peripherally (≥30° eccentricity) centered. Last three rows: cells with visual receptive fields centered in the upper or lower visual field, or along the horizontal meridian (HM).

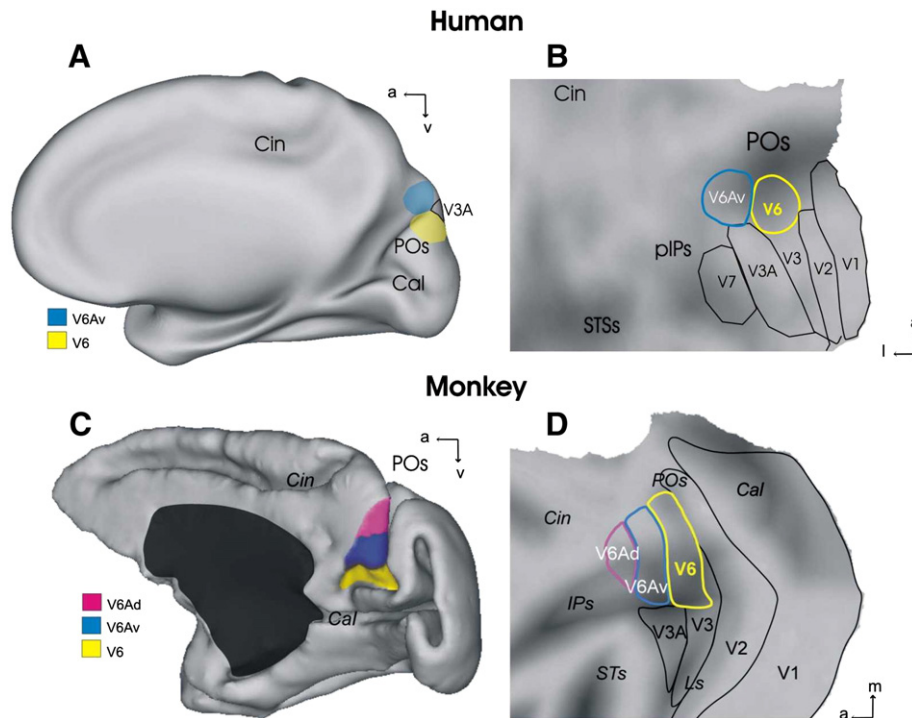|	V6Av		V6Ad	
Low-level cells	397	(69%)	134	(46%)
High-level cells	180	(31%)	158	(54%)
<30° eccentricity	92	(24%)	64	(49%)
≥30° eccentricity	294	(76%)	67	(51%)
Upper visual field	31	(8%)	24	(20%)
Lower visual field	331	(90%)	88	(73%)
HM	8	(2%)	8	(7%)

Human

Monkey

Fig. 10. Brain location of V6Av (blue) and V6 (yellow) areas in humans (A and B) and macaque monkeys (C and D). A medial view of the inflated surface (left column) and a flat map of the posterior brain (right column) are shown. A and C show the typical topographical arrangement of areas V6Av, and V6 along the POS. B and D show the spatial relationship among areas V6Av, V6, and other early visual areas. C and D show the location of macaque area V6Ad. The newly defined human area V6Av adjoins the anterior border of area V6 and the medial of area V3A (A and B), exactly as in the macaque monkey (D). The location and topography of cortical areas is based on wide-field retinotopy and functional scans in humans and on retinotopic and functional properties of single neurons in monkeys (Gamberini et al., 2011). Light and dark gray indicate gyri and sulci. Main labeled sulci: Cal, calcarine; POs, parieto-occipital sulcus; Cin, cingulate sulcus; IPS, intraparietal sulcus; STs, superior temporal sulcus.

orientation. For comparison, we analyzed the fMRI responses in neighboring area V6. These data reveal that human V6A responds to pointing movements, as both sectors of macaque V6A do (Gamberini et al., 2011); area V6, by contrast, does not respond, as is the case in macaque, further strengthening the case for the homology. Note that during the pointing tasks, subjects were not able to see their button box response movements. Thus, the pointing responses observed in area V6A were not due to the moving hand directly stimulating the lower visual field, and were instead motor-related responses.

Comparison with previous human studies

While there are no previous detailed studies of retinotopy in human V6A, a number of other neuroimaging studies have reported that the medial parieto-occipital cortex responds to pointing (Connolly et al., 2003; Simon et al., 2002; Tosoni et al., 2008) as well as to reaching and grasping movements (Beurze et al., 2007, 2009; Cavina-Pratesi et al., 2010; Filimon et al., 2007, 2009; Galati et al., 2011; Vesia et al., 2010). Also electrophysiological studies have demonstrated EEG activity in the medial parietal cortex in response to reaching movements (e.g., Bozzacchi et al., 2012). Moreover, lesions of this region disrupt visually guided arm movements toward peripheral targets (i.e., optic ataxia; Karnath and Perenin, 2005; McIntosh et al., 2011; Striemer et al., 2007, 2009).

Although it is well established that pointing execution involves activation of medial parietal cortex, one difficulty in synthesizing the data is the large variety of areal names that different authors have attributed to their medial parietal activations. Some previous studies have reported two distinct activation foci for pointing and reaching movements in the medial parietal cortex: one anterior, along the IPS, and another posterior, in the vicinity of the POs (preCUN and PO: Beurze et al., 2007; aPCU and POS: Filimon et al., 2009; aPRR and pPRR: Tosoni et al., 2008; MD and MP: Galati et al., 2011).

Other studies have reported one large activation region encompassing both foci (the human parietal reach region, hPRR: Connolly et al., 2003). Finally, others have reported only an anterior (Astafiev et al., 2003; Fernandez-Ruiz et al., 2007; Hagler et al., 2007) or only a posterior activation (Beurze et al., 2009; Cavina-Pratesi et al., 2010). Human V6A as defined in the present study likely corresponds to the posterior reaching regions described in the other studies (PO: Beurze et al., 2007; sPOS: Filimon et al., 2009; pPRR: Tosoni et al., 2008; SPOC: Gallivan et al., 2009; pSPOC: Cavina-Pratesi et al., 2010; Rossit et al., 2013; MP: Galati et al., 2011). It falls within a small posterior part of the territory of the original human parietal reach region (Connolly et al., 2003).

Single-unit data vs. human fMRI

The eccentricity data reveals that both macaque and human V6A have an over-representation of the periphery. However, while individual monkey V6A neurons represent the central 30° of the visual field (Fig. 9D), human V6A only responds in mapping experiments when the eccentricity of the visual stimuli is higher than 30° (Fig. 5). A possible explanation for this discrepancy could be that the region we call human V6A actually corresponds only to the ventral part of macaque V6A – V6Av – which responds better than V6Ad to 'low level' visual stimuli (Fig. 9C) and mostly represent the periphery (Fig. 9D). The retinotopic mapping stimuli might be less effective for 'high-level' neurons in a putative human V6Ad; and the fewer cells activated there would likely be activated by both central and peripheral stimuli (see Fig. 9D), further weakening the phase-encoded BOLD signal, which effectively subtracts out non-retinotopic activations. This could explain why we did not find V6A activations from stimulating the central 30°. Since on the basis of the monkey data, we could predict that the human V6Av, but not V6, is activated by pointing movement, as actually is the case in our fMRI experiment (Figs. 8B–C), the monkey data led to

the consideration that the lower-field-only region found here in humans is likely the homologue of monkey area V6Av.

Conclusions

The identification of human V6A extends our inventory of early visual areas in humans. Fig. 10A shows the location of the newly identified human area V6Av in a 3D semi-inflated brain. The 3D reconstruction enables to properly position the new region with respect to nearby areas V6 and V3A, which are respectively posterior and postero-lateral to V6Av. Fig. 10B shows the area V6Av on a flat map of the posterior portion of the brain together with other early visual areas mapped using wide-field retinotopic stimuli.

Figs. 10C and D compare the location of macaque area V6Av with respect to areas V6Ad, V6 and the other nearby cortical areas. A comparison between the flattened maps in Figs. 10B and D emphasizes the similarity in topographical organization and neighbor relationships of area V6Av across the two species. In macaque (Fig. 10D), V6Av abuts on area V6 posteriorly, V3A laterally, and V6Ad anteriorly. In human (Fig. 10B), the lower-field-only region (putative V6Av; blue outline) abuts V6 posteriorly, V3A laterally, and a visually poorly-responsive region anteriorly (where retinotopy is inconsistent). In both cases there are two sectors within V6A, one more sensitive to visual stimulation, V6Av, touching V6, and another, less visually responsive but more strongly reach-related just anterior to V6Av that likely corresponds to macaque V6Ad.

Acknowledgments

Conflict of interest

We have no conflict of interest to declare.

References

Astafiev, S.V., Shulman, G.L., Stanley, C.M., Snyder, A.Z., Van Essen, D.C., Corbetta, M., 2003. Functional organization of human intraparietal and frontal cortex for attending, looking, and pointing. J. Neurosci. 23, 4689–4699.

Beurze, S.M., de Lange, F.P., Toni, I., Medendorp, W.P., 2007. Integration of target and effector information in the human brain during reach planning. J. Neurophysiol. 97, 188–199.

Beurze, S.M., de Lange, F.P., Toni, I., Medendorp, W.P., 2009. Spatial and effector processing in the human parietofrontal network for reaches and saccades. J. Neurophysiol. 101, 3053–3062.

Bozzacchi, C., Giusti, M.A., Pitzalis, S., Spinelli, D., Di Russo, F., 2012. Awareness affects motor planning for goal-oriented actions. Biol. Psychol. 89 (2), 503–514.

Brewer, A.A., Press, W.A., Logothetis, N.K., Wandell, B.A., 2002. Visual areas in macaque cortex measured using functional magnetic resonance imaging. J. Neurosci. 22, 10416–10426.

Cavina-Pratesi, C., Monaco, S., Fattori, P., Galletti, C., McAdam, T.D., 2010. Functional magnetic resonance imaging reveals the neural substrates of arm transport and grip formation in reach-to-grasp actions in humans. J. Neurosci. 30, 10306–10323.

Connolly, J.D., Andersen, R.A., Goodale, M.A., 2003. FMRI evidence for a 'parietal reach region' in the human brain. Exp. Brain Res. 153, 140–145.

Crossland, M.D., Morland, A.B., Feely, M.P., von dem Hagen, E., Rubin, G.S., 2008. The effect of age and fixation instability on retinotopic mapping of primary visual cortex. Invest. Ophthalmol. Vis. Sci. 49 (8).

Dale, A.M., Fischl, B., Sereno, M.I., 1999. Cortical surface-based analysis. I. Segmentation and surface reconstruction. Neuroimage 9, 179–194.

DeYoe, E.A., Bandettini, P., Neitz, J., Miller, D., Winans, P., 1994. Functional magnetic resonance imaging (FMRI) of the human brain. J. Neurosci. Methods 54, 171–187.

DeYoe, E.A., Carman, G.J., Bandettini, P., Glickman, S., Wieser, J., Cox, R., Miller, D., Neitz, J., 1996. Mapping striate and extrastriate visual areas in human cerebral cortex. Proc. Natl. Acad. Sci. U. S. A. 93, 2382–2386.

Di Russo, F., Pitzalis, S., Spinelli, D., 2003. Fixation stability and saccadic latency in elite shooters. Vision Res. 43, 1837–1845.

Engel, S.A., Rumelhart, D.E., Wandell, B.A., Lee, A.T., Glover, G.H., Chichilnisky, E.J., Shadlen, M.N., 1994. fMRI of human visual cortex. Nature 369, 525.

Engel, S.A., Glover, G.H., Wandell, B.A., 1997. Retinotopic organization in human visual cortex and the spatial precision of functional MRI. Cereb. Cortex 7, 181–192.

Fattori, P., Gamberini, M., Kutz, D.F., Galletti, C., 2001. 'Arm-reaching' neurons in the parietal area V6A of the macaque monkey. Eur. J. Neurosci. 13 (12), 2309–2313.

Fattori, P., Kutz, D.F., Breveglieri, R., Marzocchi, N., Galletti, C., 2005. Spatial tuning of reaching activity in the medial parieto-occipital cortex (area V6A) of macaque monkey. Eur. J. Neurosci. 22 (4), 956–972.

Fattori, P., Breveglieri, R., Marzocchi, N., Filippini, D., Bosco, A., Galletti, C., 2009a. Hand orientation during reach-to-grasp movements modulates neuronal activity in the medial posterior parietal area V6A. J. Neurosci. 29 (6), 1928–1936.

Fattori, P., Pitzalis, S., Galletti, C., 2009b. The cortical visual area V6 in macaque and human brains. J. Physiol. Paris 103, 88–97.

Fattori, P., Raos, V., Breveglieri, R., Bosco, A., Marzocchi, N., Galletti, C., 2010. The dorsomedial pathway is not just for reaching: grasping neurons in the medial parieto-occipital cortex of the macaque monkey. J. Neurosci. 30 (1), 342–349.

Fernandez-Ruiz, J., Goltz, H.C., DeSouza, J.F., Vilis, T., Crawford, J.D., 2007. Human parietal "reach region" primarily encodes intrinsic visual direction, not extrinsic movement direction, in a visual motor dissociation task. Cereb. Cortex 17, 2283–2292.

Filimon, F., Nelson, J.D., Hagler, D.J., Sereno, M.I., 2007. Human cortical representations for reaching: mirror neurons for execution, observation, and imagery. Neuroimage 37, 1315–1328.

Filimon, F., Nelson, J.D., Huang, R.S., Sereno, M.I., 2009. Multiple parietal reach regions in humans: cortical representations for visual and proprioceptive feedback during on-line reaching. J. Neurosci. 29, 2961–2971.

Fischer, E., Bulthoff, H.H., Logothetis, N.K., Bartels, A., 2012. Human areas V3A and V6 compensate for self-induced planar visual motion. Neuron 73, 1228–1240.

Fischl, B., Sereno, M.I., Dale, A.M., 1999a. Cortical surface-based analysis. II. Inflation, flattening, and a surface-based coordinate system. Neuroimage 9, 195–207.

Fischl, B., Sereno, M.I., Tootell, R.B., Dale, A.M., 1999b. High-resolution intersubject averaging and a coordinate system for the cortical surface. Hum. Brain Mapp. 8, 272–284.

Galati, G., Committeri, G., Pitzalis, S., Pelle, G., Patria, F., Fattori, P., Galletti, C., 2011. Intentional signals during saccadic and reaching delays in the human posterior parietal cortex. Eur. J. Neurosci. 34 (11), 1871–1885.

Galletti, C., Fattori, P., Battaglini, P.P., Shipp, S., Zeki, S., 1996. Functional demarcation of a border between areas V6 and V6A in the superior parietal gyrus of the macaque monkey. Eur. J. Neurosci. 8, 30–52.

Galletti, C., Fattori, P., Gamberini, M., Kutz, D.F., 1999a. The cortical visual area V6: brain location and visual topography. Eur. J. Neurosci. 11, 3922–3936.

Galletti, C., Fattori, P., Kutz, D.F., Gamberini, M., 1999b. Brain location and visual topography of cortical area V6A in the macaque monkey. Eur. J. Neurosci. 11, 575–582.

Galletti, C., Kutz, D., Gamberini, M., Breveglieri, R., Fattori, P., 2003. Role of the medial parieto-occipital cortex in the control of reaching and grasping movements. Exp. Brain Res. 153, 158–170.

Gallivan, J.P., Cavina-Pratesi, C., Culham, J.C., 2009. Is that within reach? fMRI reveals that the human superior parieto-occipital cortex encodes objects reachable by the hand. J. Neurosci. 29, 4381–4391.

Gamberini, M., Galletti, C., Bosco, A., Breveglieri, R., Fattori, P., 2011. Is the medial posterior parietal area V6A a single functional area? J. Neurosci. 31 (13), 5145–5157.

Hadjikhani, N., Liu, A.K., Dale, A.M., Cavanagh, P., Tootell, R.B., 1998. Retinotopy and color sensitivity in human visual cortical area V8. Nat. Neurosci. 1 (3), 235–241.

Hagler Jr., D.J., Sereno, M.I., 2006. Spatial maps in frontal and prefrontal cortex. Neuroimage 29, 567–577.

Hagler Jr., D.J., Riecke, L., Sereno, M., 2007. Parietal and superior frontal visuospatial maps activated by pointing and saccades. Neuroimage 35, 1562–1577.

Karnath, H.O., Perenin, M.T., 2005. Cortical control of visually guided reaching: evidence from patients with optic ataxia. Cereb. Cortex 15 (10), 1561–1569.

Kwong, K.K., Belliveau, J.W., Chesler, D.A., Goldberg, I.E., Weisskoff, R.M., Poncelet, B.P., Kennedy, D.N., Hoppel, B.E., Cohen, M.S., Turner, R., Cheng, H.M., Brady, T.J., Rosen, B.R., 1992. Dynamic magnetic resonance imaging of human brain activity during primary sensory stimulation. Proc. Natl. Acad. Sci. U. S. A. 89 (12), 5675–5679.

Luppino, G., Ben Hamed, S., Gamberini, M., Matelli, M., Galletti, C., 2005. Occipital (V6) and parietal (V6A) areas in the anterior wall of the parieto-occipital sulcus of the macaque: a cytoarchitectonic study. Eur. J. Neurosci. 21, 3056–3076.

McIntosh, R.D., Mulroue, A., Blangero, A., Pisella, L., Rossetti, Y., 2011. Correlated deficits of perception and action in optic ataxia. Neuropsychologia 49 (1), 131–137.

Monaco, S., Cavina-Pratesi, C., Sedda, A., Fattori, P., Galletti, C., Culham, J.C., 2011. Functional magnetic resonance adaptation reveals the involvement of the dorsomedial stream in hand orientation for grasping. J. Neurophysiol. 106 (5), 2248–2263.

Oldfield, R.C., 1971. The assessment and analysis of handedness: the Edinburgh inventory. Neuropsychologia 9, 97–113.

Pitzalis, S., Galletti, C., Huang, R.-S., Patria, F., Committeri, G., Galati, G., Fattori, P., Sereno, M.I., 2006. Wide-field retinotopy defines human cortical visual area V6. J. Neurosci. 26, 7962–7973.

Pitzalis, S., Sereno, M.I., Committeri, G., Fattori, P., Galati, G., Patria, F., Galletti, C., 2010. Human V6: the medial motion area. Cereb. Cortex 20 (2), 411–424.

Pitzalis, S., Fattori, P., Galletti, C., 2012. The functional role of the medial motion area V6. Front. Behav. Neurosci. 6, 91.

Pitzalis, S., Bozzacchi, C., Bultrini, A., Fattori, P., Galletti, C., Di Russo, F., 2013a. Parallel motion signals to the medial and lateral motion areas V6 and MT+. Neuroimage 67, 89–100.

Pitzalis, S., Sdoia, S., Bultrini, A., Committeri, G., Di Russo, F., Fattori, P., Galletti, C., Galati, G., 2013b. Selectivity to translational egomotion in human brain motion areas. PLoS One 8 (4), e60241. http://dx.doi.org/10.1371/journal.pone.0060241.

Rossit, S., McAdam, T., McLean, D.A., Goodale, M.A., Culham, J.C., 2013. fMRI reveals a lower visual field preference for hand actions in human superior parieto-occipital cortex (SPOC) and precuneus. Cortex. http://dx.doi.org/10.1016/j.cortex.2012.12.014 (Jan 8, pii: S0010-9452(12)00371-1, Epub ahead of print).

Sereno, M.I., 1998. Brain mapping in animals and humans. Curr. Opin. Neurobiol. 8, 188–194.

Sereno, M.I., Tootell, R.B.H., 2005. From monkeys to humans: what do we now know about brain homologies? Curr. Opin. Neurobiol. 15, 135–144.

Sereno, M.I., McDonald, C.T., Allman, J.M., 1994. Analysis of retinotopic maps in extrastriate cortex. Cereb. Cortex 4, 601–620.

Sereno, M.I., Dale, A.M., Reppas, J.B., Kwong, K.K., Belliveau, J.W., Brady, T.J., Rosen, B.R., Tootell, R.B., 1995. Borders of multiple visual areas in humans revealed by functional magnetic resonance imaging. Science 268, 889–893.

Sereno, M.I., Pitzalis, S., Martinez, A., 2001. Mapping of contralateral space in retinotopic coordinates by a parietal cortical area in humans. Science 294, 1350–1354.

Simon, O., Mangin, J.F., Cohen, L., Le Bihan, D., Dehaene, S., 2002. Topographical layout of hand, eye, calculation, and language-related areas in the human parietal lobe. Neuron 33, 475–487.

Striemer, C., Blangero, A., Rossetti, Y., Boisson, D., Rode, G., Vighetto, A., Pisella, L., Danckert, J., 2007. Deficits in peripheral visual attention in patients with optic ataxia. Neuroreport 18 (11), 1171–1175.

Striemer, C., Locklin, J., Blangero, A., Rossetti, Y., Pisella, L., Danckert, J., 2009. Attention for action? Examining the link between attention and visuomotor control deficits in a patient with optic ataxia. Neuropsychologia 47 (6), 1491–1499.

Tootell, R.B., Mendola, J.D., Hadjikhani, N.K., Ledden, P.J., Liu, A.K., Reppas, J.B., Sereno, M.I., Dale, A.M., 1997. Functional analysis of V3A and related areas in human visual cortex. J. Neurosci. 17, 7076–7078.

Tosoni, A., Galati, G., Romani, G.L., Corbetta, M., 2008. Sensory-motor mechanisms in human parietal cortex underlie arbitrary visual decisions. Nat. Neurosci. 11, 1446–1453.

Van Essen, D.C., 2005. A Population-Average, Landmark- and Surface-based (PALS) atlas of human cerebral cortex. Neuroimage 28 (3), 635–662.

Van Essen, D.C., Glasser, M.F., Dierker, D., Harwell, J., Coalson, T., 2012. Parcellations and hemispheric asymmetries of human cerebral cortex analyzed on surface-based atlases. Cereb. Cortex 22 (10), 2241–2262.

Vesia, M., Prime, S.L., Yan, X., Sergio, L.E., Crawford, J.D., 2010. Specificity of human parietal saccade and reach regions during transcranial magnetic stimulation. J. Neurosci. 30 (39), 13053–13065.

Zarahn, E., Aguirre, G.K., D'Esposito, M., 1997. Empirical analyses of BOLD fMRI statistics. I. Spatially unsmoothed data collected under null-hypothesis conditions. Neuroimage 5, 179–197.